MISC Array: A New Sparse Array Design Achieving Increased Degrees of Freedom and Reduced Mutual Coupling Effect

Zhi Zheng, *Member, IEEE*, Wen-Qin Wang, *Senior Member, IEEE*, Yangyang Kong and Yimin D. Zhang, *Fellow, IEEE*

***Abstract*— Recently, nested and coprime arrays have attracted considerable interest due to their capability of providing increased array aperture, enhanced degrees of freedom (DOFs), and reduced mutual coupling effect compared to uniform linear arrays (ULAs). These features are critical to improving the performance of DOA estimation and adaptive beamforming. In this paper, a new sparse array configuration based on the maximum inter-element spacing constraint (MISC) is proposed. The MISC array configuration generally consists of three sparse ULAs plus two separate sensors that are appropriately placed. The MISC array configurations are designed based on the inter-element spacing set, which, for a given number of sensors, is uniquely determined by a closed-form expression. We also derive closed-form expressions for the number of uniform DOFs of the MISC arrays with any number of sensors. Compared with the existing sparse arrays, the MISC array enjoys two important advantages, namely, providing a higher number of DOFs and reducing the mutual coupling effects. Numerical simulations are conducted to verify the superiority of the MISC array over other sparse arrays.**

***Index Terms*— Sparse arrays, MISC arrays, degrees of freedom (DOFs), mutual coupling, direction-of-arrival estimation.**

I. Introduction

Array signal processing is a fundamental technology used in various applications such as radar, sonar, navigation, wireless communications, electronic surveillance and radio astronomy [1], [2]. Key benefits of using sensor arrays include spatial selectivity and the capability to mitigate interference and improve signal quality. The most commonly used sensor arrays are conventional uniform linear arrays (ULAs), where the inter-element spacing is constant and is not more than half wavelength to avoid spatial aliasing. However, the number of degrees of freedom (DOFs) of conventional ULAs is only linear to the number of sensors. For an N-sensor ULA, the traditional subspace-based methods [3], [4] can resolve up to $N-1$ sources. To increase the number of DOFs within the conventional ULA framework, additional sensors are required, thus leading to a high complexity that may be impractical or infeasible. Conventional ULAs also suffer from severe mutual coupling effects between array sensors.

On the other hand, nonuniform linear arrays (NLAs) (also referred to as sparse arrays) offer an attractive solution to these problems. By vectorizing the covariance matrix of the received array signal, an N-sensor sparse array provides $\mathcal{O}(N^2)$ consecutive virtual sensors in the difference coarray. In other words, up to $\mathcal{O}(N^2)$ uncorrelated sources can be identified using N physical sensors [5]. This implies a significantly increased number of DOFs compared to traditional ULAs. Moreover, mutual coupling effects may also be reduced due to the larger inter-element spacing in sparse arrays [6].

One of the most well known sparse array configurations is the minimum redundancy array (MRA). For a given number of physical sensors, the MRA maximizes the number of consecutive virtual sensors in the difference coarray [7]. It has been shown that, by constructing an augmented covariance matrix [8], [9], the MRA is the optimum geometry to achieve the maximum difference coarray aperture for a given number of sensors. Another well-known sparse array is the minimum hole array (MHA) (also known as the Golomb array) that minimizes the number of holes in the difference coarray [10]. Although MRAs and MHAs are shown to be effective to increase the number of achievable DOFs, they have no closed-form expressions for the sensor positions and the number of achievable DOFs. As a result, designing such arrays for an arbitrary number of sensors is difficult [11]. Such shortcomings restrict their applications in practice.

Recently, the development of sparse arrays, such as nested arrays [12], [13] and coprime arrays [14], [15], has invited researchers to revisit this topic because such array configurations can be systematically designed and their numbers of achievable DOFs can be analytically provided with closed-form expressions [16]–[45].

The nested array, which is obtained by combining two or more ULAs with increased inter-element spacing, can overcome the shortcomings of MRAs and MHAs and, at the same time, provide $\mathcal{O}(N^2)$ DOFs with only N physical sensors [13]. The two-level nested array refers to a structure consisting of two ULAs, whose resulting difference coarray is a filled ULA (i.e., hole-free). However, for a given number

The work of Z. Zheng, W. Wang, and Y. Kong was supported in part by the National Natural Science Foundation of China under Grant 61571081, by the Sichuan Science and Technology Program under Grant 2018RZ0141, by the Sichuan Applied Basic Research Program under Grant 19YYJC0100, by the Key Project of Sichuan Education Department of China under Grant 18ZA0221, by the Guangdong Natural Science Foundation of China under Grant 2018A0303130064, and by the Fundamental Research Funds for the Central Universities of China under Grant 2672018ZYGX2018J003.

Z. Zheng, W. Wang and Y. Kong are with the School of Information and Communication Engineering, University of Electronic Science and Technology of China, Chengdu 611731, China (e-mail: zz@uestc.edu.cn; wqwang@uestc.edu.cn; 18623353803@163.com).

Y. D. Zhang is with the Department of Electrical and Computer Engineering, Temple University, Philadelphia, PA, USA 19122 (e-mail: ydzhang@temple.edu).

of physical sensors, the number of DOFs offered by a nested array is smaller than that of the MRA. Although nested arrays with more than two levels can provide a higher number of DOFs, their difference coarrays are not necessarily a hole-free ULA. In [16], an improved nested array is proposed via increasing the inter-element spacing of the outer ULA and adding an additional sensor. The new nested array enjoys all the excellent properties of the two-level nested array and can provide a higher number of DOFs. Two-dimensional extensions of nested arrays are provided in [17], [18].

On the other hand, due to a densely packed ULA in the physical array, the nested array still remains sensitive to the mutual coupling effects between elements [46]. In [19], [20], a sparse array configuration, referred to as the (second-order) super nested array, is introduced which maintains the key advantages of the existing nested array families, i.e., the sensor locations have a closed-form expression, and the difference coarray is hole-free. At the same time, the super nested array avoids some of the disadvantages of the conventional nested array. In particular, the mutual coupling effect is substantially reduced compared to the nested arrays. Super nested arrays are designed by rearranging the dense ULA part of a nested array in such a way that the coarray remains unchanged, but mutual coupling effect is reduced by reducing the number of elements with small inter-element spacing. In [21], [22], a generalization of super nested arrays, referred to as the Qth-order super nested array (where Q is generally larger than 2), is introduced. It keeps the desired properties of the second-order super nested array while further reducing the mutual coupling effects. In [23], a new nested array named augmented nested array (ANA) is proposed by splitting the dense ULA of a nested array into two or four parts, which can be relocated at the two sides of the sparse ULA of a nested array. Depending on how the splitting takes place, four different ANAs, i.e., ANAI-1, ANAI-2, ANAII-1 and ANAII-2, are derived. These ANAs provide a higher number of DOFs compared with the existing nested and super nested array configurations. However, they also have some disadvantages. ANAI-1 and ANAI-2 cannot significantly reduce the mutual coupling effect. Although ANAII-1 and ANAII-2 are more effective against mutual coupling, the array splitting has to satisfy complicated conditions in order to obtain hole-free difference coarrays.

Another attractive sparse array is the coprime array. The prototype coprime array [15] consists of two ULAs where one ULA has M sensors with $N\lambda/2$ inter-element spacing, while the other ULA has N sensors with $M\lambda/2$ inter-element spacing, where M and N are a pair of coprime integers and λ is the signal wavelength. Compared with the nested array, the coprime array can further reduce mutual coupling effects between elements. However, given the same number of array sensors, the number of DOFs offered by a coprime array is generally lower than that by a nested array counterpart. To further increase the number of DOFs, an extended coprime array was proposed in [24] by doubling the number of sensors in one ULA. By using $2M + N - 1$ sensors, its difference coarray can obtain consecutive lags between $-MN - N + 1$ and $MN + N - 1$.

In [25], [26], the coprime array is generalized by performing two operations. The first operation is compressing the inter-element spacing of one subarray in the coprime array, which yields a coprime array with compressed inter-element spacing (CACIS). The CACIS generally increases the number of both consecutive and unique lags. However, the minimum inter-element spacing in CACIS remains unit spacing, and there are still a considerable number of overlapping self- and cross-lags. To overcome these issues, the second operation introduced in [25], [26] is to displace one subarray in the coprime array so that the resulting coprime array with displaced subarrays (CADiS) provides a much larger minimum inter-element spacing, a larger array aperture, and a higher number of unique lags. Note that coprime arrays can be arranged into a multi-level design [27], [28]. However, they are generally not attractive in providing a high number of consecutive and unique lags as compared to the nested array and the CACIS.

In this paper, we introduce a new array configuration based on the maximum inter-element spacing constraint (MISC) criterion. The MISC array is designed in terms of the inter-element spacing set, which is given in a closed-form expression as a function of the number of sensors. Generally, the MISC array configuration consists of three sparse ULAs plus two separate sensors which are set apart with an appropriate spacing. The MISC array possesses all the desired properties of the nested array, such as hole-free difference coarrays and a large coarray aperture. For a given number of sensors, the sensor locations of the MISC array are uniquely determined by a closed-form expression and the number of achievable DOFs is analytically presented as well. More importantly, compared with the nested array and the coprime array with the same number of sensors, the MISC array configuration offers a higher number of DOFs and reduced mutual coupling effects. Numerical results demonstrate its superiority in comparison to different existing sparse array configurations.

The rest of this paper is organized as follows. Some necessary preliminaries are introduced in Section II. In Section III, we present the MISC array concept, including its design rules and array structure, the number of DOFs, and the weight functions. Numerical results are provided in Section IV to demonstrate the superiority of the proposed MISC arrays. Finally, conclusions are drawn in Section V.

Throughout this paper, bold lower-case (upper-case) characters represent vectors (matrices). In particular, $\mathbf{I}_N$ denotes the $N \times N$ identity matrix. The superscripts $*$, T and H denote the complex conjugate, transpose and conjugate transpose, respectively. $E\{\cdot\}$ is the statistical expectation operator and $\mathrm{vec}(\cdot)$ represents the vectorization operator that turns a matrix into a vector by stacking all columns on top of the other. $\langle\cdot\rangle_{n_1,n_2}$ denotes the (n_1, n_2)th entry of a matrix; $\mathrm{diag}(\mathbf{a})$ denotes a diagonal matrix that uses the elements of $\mathbf{a}$ as its diagonal elements. The symbol $\otimes$ denotes the Kronecker product, $\%$ denotes the remainder, $\|\cdot\|_F$ denotes the Frobenius norm, and $\lfloor\cdot\rfloor$ is the integral part of the rational number in the square brackets.

II. PRELIMINARIES

A. Difference Coarray Signal Model

Consider an N-sensor nonuniform linear array, whose sensor positions are given by $n_i d$, where n_i belongs to an integer set $\mathbb{S} = \{n_i, i = 1, 2, \ldots, N\}$ and $d = \lambda/2$ denotes the minimum distance between sensors, with λ being the wavelength of the incoming wave. Assume that K far-field, uncorrelated narrowband signals impinge on the array from distinct directions $\{\theta_1, \theta_2, \ldots, \theta_K\}$ with powers $\{\sigma_1^2, \sigma_2^2, \ldots, \sigma_K^2\}$. The signal received by the array at time t is modeled as

$$\mathbf{x}(t) = \sum_{k=1}^{K} \mathbf{a}(\bar{\theta}_k) s_k(t) + \mathbf{n}(t) = \mathbf{A}\mathbf{s}(t) + \mathbf{n}(t) \tag{1}$$

where $\mathbf{s}(t) = [s_1(t), s_2(t), \ldots, s_K(t)]^T$ is the signal waveform vector. The elements of $\mathbf{n}(t) \sim \mathcal{CN}(0, \sigma_n^2 \mathbf{I}_N)$ are assumed to be independent and identically distributed (i.i.d.) additive white Gaussian noise, and are uncorrelated from the sources. $\mathbf{A} = [\mathbf{a}(\bar{\theta}_1), \mathbf{a}(\bar{\theta}_2), \ldots, \mathbf{a}(\bar{\theta}_K)]$ is the $N \times K$ array manifold matrix, and $\mathbf{a}(\bar{\theta}_k)$ is the steering vector of the array corresponding to the kth signal, given by

$$\mathbf{a}(\bar{\theta}_k) = [e^{j2\pi n_1 \bar{\theta}_k}, e^{j2\pi n_2 \bar{\theta}_k}, \ldots, e^{j2\pi n_N \bar{\theta}_k}]^T \tag{2}$$

with $\bar{\theta}_k = (d/\lambda)\sin\theta_k$ denoting the normalized DOA. We obtain $-1/2 \le \bar{\theta}_k \le 1/2$.

The theoretical covariance matrix of $\mathbf{x}(t)$ can be expressed as

$$\begin{aligned} \mathbf{R}_{\mathbf{xx}} &= E\{\mathbf{x}(t)\mathbf{x}^H(t)\} = \mathbf{A}\mathbf{R}_{\mathbf{ss}}\mathbf{A}^H + \sigma_n^2 \mathbf{I}_N \\ &= \sum_{k=1}^{K} \sigma_k^2 \mathbf{a}(\bar{\theta}_k)\mathbf{a}^H(\bar{\theta}_k) + \sigma_n^2 \mathbf{I}_N \end{aligned} \tag{3}$$

where $\mathbf{R}_{\mathbf{ss}} = E\{\mathbf{s}(t)\mathbf{s}^H(t)\} = \mathrm{diag}([\sigma_1^2, \ldots, \sigma_K^2])$ is the source covariance matrix, and σ_n^2 represents the noise variance.

Since the theoretical $\mathbf{R}_{\mathbf{xx}}$ is unavailable in practice, it is usually replaced by the sample covariance matrix

$$\hat{\mathbf{R}}_{\mathbf{xx}} = \frac{1}{T} \sum_{t=1}^{T} \mathbf{x}(t)\mathbf{x}^H(t) \tag{4}$$

where T denotes the number of snapshots.

Vectorizing $\hat{\mathbf{R}}_{\mathbf{xx}}$ yields

$$\begin{aligned} \mathbf{z} = \mathrm{vec}(\hat{\mathbf{R}}_{\mathbf{xx}}) &= \mathrm{vec}\left[\sum_{k=1}^{K} \sigma_k^2 \mathbf{a}(\bar{\theta}_k)\mathbf{a}^H(\bar{\theta}_k)\right] + \sigma_n^2 \mathbf{1}_n \\ &= \mathbf{B}\mathbf{p} + \sigma_n^2 \mathbf{1}_n \end{aligned} \tag{5}$$

where $\mathbf{B} = [\mathbf{b}(\bar{\theta}_1), \ldots, \mathbf{b}(\bar{\theta}_K)]$, $\mathbf{b}(\bar{\theta}_k) = \mathbf{a}^*(\bar{\theta}_k) \otimes \mathbf{a}(\bar{\theta}_k)$, $\mathbf{p} = [\sigma_1^2, \sigma_2^2, \ldots, \sigma_K^2]^T$, and $\mathbf{1}_n = \mathrm{vec}(\mathbf{I}_N) = [\mathbf{e}_1^T, \mathbf{e}_2^T, \ldots, \mathbf{e}_N^T]^T$ with $\mathbf{e}_i$ being a column vector of all zeros except a 1 at the ith position. Comparing (1) with (5), the vector $\mathbf{z}$ can be viewed as the received data from a coherent source signal vector $\mathbf{p}$ with a single snapshot, and $\sigma_n^2 \mathbf{1}_n$ becomes a deterministic noise term. The distinct rows of $\mathbf{B}$ behave like the manifold of a virtual array with an extended aperture whose sensor positions are given by the difference set $\mathbb{D}$ in Definition 1. This virtual array is called the difference coarray of the original array [5]. Assuming that $\mathbb{U} = [-L_u, L_u]$ is the consecutive segment of $\mathbb{D}$, the corresponding measurements can be rearranged to form a new $(2L_u + 1) \times 1$ vector $\mathbf{z}_{\mathbb{U}}$ expressed as

$$\mathbf{z}_{\mathbb{U}} = \mathbf{J}\mathbf{z} = \mathbf{B}'\mathbf{p} + \sigma_n^2 \mathbf{1}'_n \tag{6}$$

where $\mathbf{J}$ denotes a $(2L_u + 1) \times N^2$ selection matrix, $\mathbf{B}'$ is a $(2L_u + 1) \times K$ manifold matrix corresponding to the consecutive virtual ULA $\mathbb{U}$, and $\mathbf{1}'_n$ is a $(2L_u + 1) \times 1$ vector of all zeros except a 1 at the $(L_u + 1)$th position.

Definition 1 (Difference Coarray): For a sparse array specified by a sensor position set $\mathbb{S}$, its difference coarray $\mathbb{D}$ is defined as

$$\mathbb{D} = \{n_1 - n_2 | n_1, n_2 \in \mathbb{S}\} \tag{7}$$

Definition 2 (Degrees of Freedom [20]): The number of degrees of freedom of a sparse array $\mathbb{S}$ is the cardinality of its difference coarray $\mathbb{D}$.

Definition 3 (Uniform DOFs [20]): Given a sparse array $\mathbb{S}$, let $\mathbb{U}$ denote the maximum consecutive segment of its difference coarray $\mathbb{D}$. The cardinality of $\mathbb{U}$ is referred to as the number of "uniform DOFs" of $\mathbb{S}$.

B. Mutual Coupling

The received signal vector in (1) does not consider the mutual coupling between the physical elements. In practical application, however, the mutual coupling effect between the elements with small separation cannot be neglected. After incorporating the mutual coupling effect, (1) can be rewritten as

$$\mathbf{x}(t) = \mathbf{C}\mathbf{A}\mathbf{s}(t) + \mathbf{n}(t) \tag{8}$$

where $\mathbf{C}$ is the $N \times N$ mutual coupling matrix. Note that the coupling-free model (1) can be regarded as a special case of (8), where $\mathbf{C}$ is an identity matrix.

In general, the expression for $\mathbf{C}$ is rather complicated [20], [23]. In the ULA configuration, $\mathbf{C}$ can be approximated by a B-banded symmetric Toeplitz matrix as follows [47]–[54]:

$$\langle \mathbf{C} \rangle_{n_1, n_2} = \begin{cases} c_{|n_1 - n_2|}, & \text{if } |n_1 - n_2| \le B, \\ 0, & \text{otherwise}, \end{cases} \tag{9}$$

where $n_1, n_2 \in \mathbb{S}$ and $c_0, c_1, \ldots, c_B$ are coupling coefficients satisfying $c_0 = 1 > |c_1| > |c_2| > \cdots > |c_B|$. It is assumed that the magnitudes of coupling coefficients are inversely proportional to their sensor separations, i.e., $|c_k/c_\ell| = \ell/k$ for $k, \ell > 0$ [47]. To evaluate the mutual coupling effect, the weight function and coupling leakage are usually used.

Definition 4 (Weight Function): The weight function $w(l)$ of an array $\mathbb{S}$ is defined as the number of sensor pairs that lead to coarray index l. Namely,

$$w(l) = |\{(n_1, n_2) \in \mathbb{S}^2 | n_1 - n_2 = l\}|, \quad l \in \mathbb{D}. \tag{10}$$

Note that the weight function $w(l)$ for any linear array with N sensors satisfies the following properties [20]:

$$w(0) = N, \ \sum_{l \in \mathbb{D}} w(l) = N^2, \ \ w(l) = w(-l). \tag{11}$$

Definition 5 (Coupling Leakage): For a given number of sensors, the coupling leakage is defined as the energy ra-

tio [20]:

$$L = \frac{\|\mathbf{C} - \mathrm{diag}(\mathbf{C})\|_F}{\|\mathbf{C}\|_F} \tag{12}$$

where $\|\mathbf{C} - \mathrm{diag}(\mathbf{C})\|_F$ is the energy of all the off-diagonal components, which characterizes the level of mutual coupling. A small value of L implies that the mutual coupling is less significant.

III. MISC Array Concept

In this section, we will introduce *MISC arrays*, which are constructed based on maximum inter-element spacing constraint. These new array configurations have many desirable properties and advantages. First, similar to the nested and coprime arrays, their sensor locations and the achievable number of DOFs can be expressed in a closed form. In addition, the difference coarrays of MISC arrays are hole-free. This advantage is shared by the nested array family but not those based on the coprime array. Most importantly, MISC arrays possess a higher number of DOFs and less mutual coupling effects, compared to the existing sparse arrays.

A. Design Rules and Array Structure

The MISC arrays are constructed based on the given inter-element spacings for an arbitrary number of sensors. Denote P as the maximum inter-element spacing, and $\mathbb{A}$ as the associated inter-element spacing set. Then, we may use P and $\mathbb{A}$ to determine the sensor positions of MISC arrays. Specifically, P and $\mathbb{A}$ for MISC arrays are defined as:

MISC Arrays:

$$P = 2\left\lfloor \frac{N}{4} \right\rfloor + 2, \quad (N \geq 5) \tag{13}$$

$$\mathbb{A}_{\mathrm{MISC}} = \{1, P-3, \underbrace{P, \ldots, P}_{N-P}, \underbrace{2, \ldots, 2}_{\frac{P-4}{2}}, 3, \underbrace{2, \ldots, 2}_{\frac{P-4}{2}}\}. \tag{14}$$

Note in (14) that there are 6 inter-element spacing groups where 4 of them are always positive, whereas the other two may take a value of zero. Therefore, the minimum number of sensors in a MISC array is 5, i.e., $N \geq 5$. Clearly, P is an even number ($P \geq 4$) and increases as N increases.

The sensor position set corresponding to $\mathbb{A}_{\mathrm{MISC}}$ is expressed as

$$\begin{aligned}\mathbb{S}_{\mathrm{MISC}} = \{&0, 1, P-2, 2P-2, \ldots, (N-P+1)P-2,\\ &(N-P+1)P, (N-P+1)P+2, \ldots, (N-P+2)P\\ &-6, (N-P+2)P-3, (N-P+2)P-1,\\ &(N-P+2)P+1, \ldots, (N-P+3)P-7\}.\end{aligned} \tag{15}$$

The sensor locations of the MISC array configuration are shown in Fig. 1. It is clear that the sensor positions can be represented as a function of N and P. Since P is determined by N, MISC arrays have closed-form expressions for the sensor positions with respect to an arbitrary number of sensors.

In an MISC array, the associated $\mathbb{A}_{\mathrm{MISC}}$ is generally divided into three parts. The first part only contains two elements: 1 and $P-3$, which denote two sensors with $\lambda/2$ element spacing, and the third sensor is further separated by a spacing of $(P-3)\lambda/2$. The second part consists of $N-P$ elements of P, which corresponds to a sparse ULA with $N-P$ sensors and inter-element spacing $P\lambda/2$. The third part is a set of $P-4$ elements of 2 and one element of 3, and is symmetric about 3, which implies two sparse ULAs with $(P-4)/2$ and $(P-4)/2+1 = (P-2)/2$ sensors (the addition of 1 is due to the very last sensor), respectively, where the inter-element spacing within each ULA is λ, and the spacing between the two ULAs is $3\lambda/2$.

We compare the MISC array with the nested array [13] and the improved nested array [16]. Both the nested and the improved nested array render hole-free difference coarrays. Note that we do not compare the coprime array in this subsection because the difference array reconstructed from a coprime array is generally not hole-free and thus coprime arrays are not effective when considering coarrays with consecutive lags. P and $\mathbb{A}$ for the nested arrays and the improved nested arrays are given by

Nested Arrays:

$$P = \begin{cases} \frac{N+1}{2}, & \text{if } N \text{ is odd,} \\ \frac{N}{2}, & \text{if } N \text{ is even,} \end{cases} \tag{16}$$

$$\mathbb{A}_{\mathrm{nested}} = \{\underbrace{1, 1, \ldots, 1}_{P-1}, \underbrace{P, P, \ldots, P}_{N-P}\}. \tag{17}$$

Improved Nested Arrays:

$$P = \begin{cases} \frac{N+1}{2}+1, & \text{if } N \text{ is odd,} \\ \frac{N}{2}+1, & \text{if } N \text{ is even,} \end{cases} \tag{18}$$

$$\mathbb{A}_{\mathrm{improved}} = \{\underbrace{1, 1, \ldots, 1}_{P-2}, \underbrace{P, \ldots, P}_{N-P}, P-1\}. \tag{19}$$

It is observed that $\mathbb{A}_{\mathrm{nested}}$ and $\mathbb{A}_{\mathrm{improved}}$ contain more ones than $\mathbb{A}_{\mathrm{MISC}}$. This indicates that the MISC array is sparser than both the nested array and the improved nested array, thus is much less sensitive to mutual coupling effects.

Next, we illustrate the structure of the MISC array by two specific examples. First, we consider the special case of $N = 5$. Fig. 2(c) shows the structure of the 5-element MISC array. For comparison, the nested array and the improved nested array with the same number of sensors are plotted in Figs. 2(a) and 2(b), respectively. Accordingly, $\mathbb{A}$ for the MISC arrays and the improved nested arrays is $\{1, 1, 4, 3\}$, while $\mathbb{A}$ for the nested arrays is $\{1, 1, 3, 3\}$. For this specific case, the MISC array and the improved nested array have the same configuration with $P = 4$, while $P = 3$ for the nested array.

Another illustrative example of the 8-element MISC array configuration is shown in Fig. 3, together with the nested array and the improved nested array configurations with the same number of sensors. It can be seen that the MISC array has a larger P than the nested array and the improved nested array. Moreover, for the MISC arrays, $\mathbb{A} = \{1, 3, 6, 6, 2, 3, 2\}$, while for the nested arrays and the improved nested arrays, $\mathbb{A}$ becomes $\{1, 1, 1, 4, 4, 4, 4\}$ and $\{1, 1, 1, 5, 5, 5, 4\}$, respectively. Thus, the MISC array is sparser and has a larger array aperture

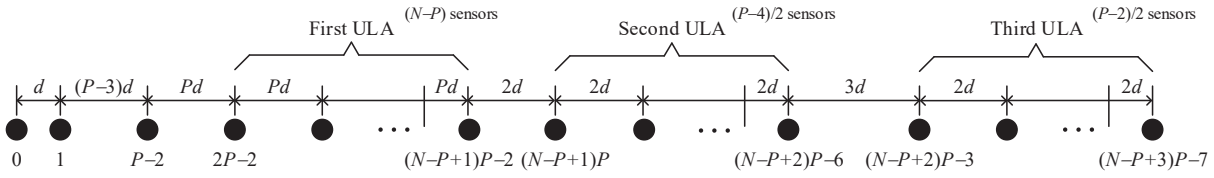

Fig. 1. The MISC array configuration.

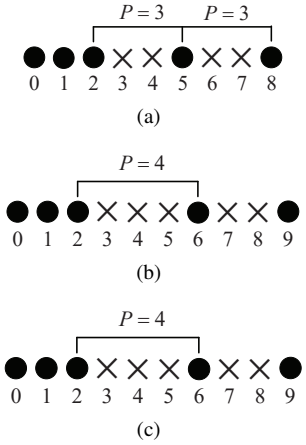

Fig. 2. The array configurations for three kinds of 5-element NLAs. (a) Nested, $N_1 = 3, N_2 = 2$. (b) Improved Nested, $N_1 = 3, N_2 = 2$. (c) MISC, $N = 5$. Bullets represent physical sensors while crosses stand for empty locations.

than the nested array and the improved nested array. Note that the MISC array yields a hole-free difference coarray, as formally described in Lemma 1.

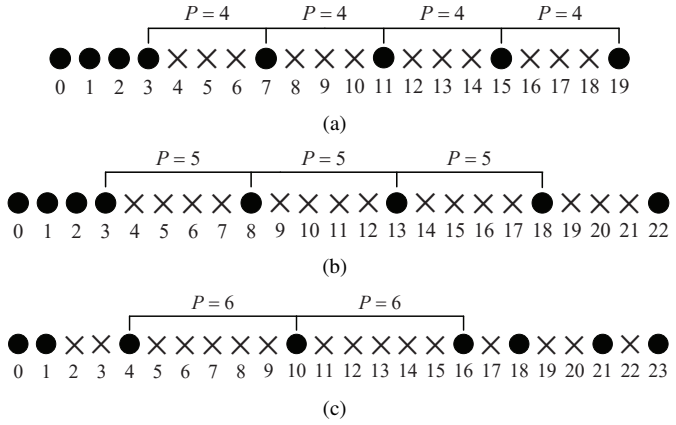

Fig. 3. The array configurations for three kinds of 8-element NLAs. (a) Nested, $N_1 = N_2 = 4$. (b) Improved Nested, $N_1 = N_2 = 4$. (c) MISC, $N = 8$. Bullets represent physical sensors while crosses stand for empty locations.

Lemma 1: The difference coarrays of MISC arrays are hole-free virtual ULAs, i.e., $\mathbb{D}_{\rm MISC} = \mathbb{U}$.

Proof: In terms of $\mathbb{S}_{\rm MISC}$, the maximum distance between the sensors is the difference between the last element and the first element, i.e., $(N-P+3)P-7$. Since $\mathbb{D}_{\rm MISC}$ is symmetric about 0, we only need to prove that its positive part $\mathbb{D}^+_{\rm MISC}$ contains the consecutive set $\mathbb{F} = \{1, 2, 3, \ldots, (N-P+3)P-7\}$.

Based on $\mathbb{S}_{\rm MISC} = \{n_i, i = 1, 2, \ldots, N\}$, we may construct the $N-1$ positive difference sets as:

$$\begin{aligned}
&\mathbb{D}_1 = \{n_2 - n_1, \ldots, n_N - n_1\},\\
&\mathbb{D}_2 = \{n_3 - n_2, \ldots, n_N - n_2\},\\
&\mathbb{D}_3 = \{n_4 - n_3, \ldots, n_N - n_3\},\\
&\cdots\cdots\cdots\cdots\cdots\\
&\mathbb{D}_{N-3} = \{n_{N-2} - n_{N-3}, n_N - n_{N-3}\},\\
&\mathbb{D}_{N-2} = \{n_{N-1} - n_{N-2}, n_N - n_{N-2}\},\\
&\mathbb{D}_{N-1} = \{n_N - n_{N-1}\}.
\end{aligned} \tag{20}$$

The above integer sets can be concretely expressed as (21), shown at the bottom of the next page.

Let $\mathbb{D}_0 = \mathbb{D}_1 \cup \mathbb{D}_2 \cup \cdots \cup \mathbb{D}_{N-1}$. The proof of $\mathbb{D}_0 \supset \mathbb{F}$ can be carried out by finding the consecutive lags $\{kP + 1, kP + 2, \ldots, (k+1)P\}$ $(0 \le k \le (N-P+2))$ from some subsets of $\mathbb{D}_0$. First, the lag $\{1, 2, \ldots, P\}$ can be obtained from $\mathbb{D}_1 \cup \mathbb{D}_2 \cup \mathbb{D}_3 \cup \mathbb{D}_{N-P+4+(P-4)/2} \cup \mathbb{D}_{N-P+4+(P-4)/2+1}$. Then, the lag $\{P+1, P+2, \ldots, 2P\}$ can be obtained from $\mathbb{D}_1 \cup \mathbb{D}_2 \cup \mathbb{D}_3 \cup \mathbb{D}_{N-P+2} \cup \mathbb{D}_{N-P+3}$. Next, the lag $\{2P + 1, 2P + 2, \ldots, 3P\}$ can be obtained from $\mathbb{D}_1 \cup \mathbb{D}_2 \cup \mathbb{D}_3 \cup \mathbb{D}_{N-P+1} \cup \mathbb{D}_{N-P+2}$, and so on. In the penultimate step, the lag $\{(N-P+1)P+1, (N-P+1)P+2, \ldots, (N-P+2)P\}$ can be obtained from $\mathbb{D}_1 \cup \mathbb{D}_2 \cup \mathbb{D}_3$. Finally, the lag $\{(N - P + 2)P + 1, (N - P + 2)P + 2, \ldots, (N - P + 3)P - 7\}$ can be obtained from $\mathbb{D}_1 \cup \mathbb{D}_2$. Since $\mathbb{F}$ consists of the lags $\{kP + 1, kP + 2, \ldots, (k+1)P\}$, we can conclude $\mathbb{D}_0 \supset \mathbb{F}$. Since $\mathbb{D}^+_{\rm MISC}$ consists of 0 and the distinct elements in $\mathbb{D}_0$, we can derive $\mathbb{D}^+_{\rm MISC} \supset \mathbb{F}$. According to the symmetry, we get $\mathbb{D}_{\rm MISC} = \{-((N - P + 3)P - 7), -((N - P + 3)P - 7) + 1, \ldots, -1, 0, 1, \ldots, (N - P + 3)P - 7\}$. Therefore, the difference coarrays of MISC arrays are hole-free ULAs, i.e., $\mathbb{D}_{\rm MISC} = \mathbb{U}$. ■

B. Uniform DOFs

From the integer set $\mathbb{S}_{\rm MISC}$, we can derive that the difference set of a MISC array is given by a consecutive set between $-(N - P + 3)P + 7$ and $(N - P + 3)P - 7$, i.e.,

$$\begin{aligned}
\mathbb{D}_{\rm MISC} = \{&-(N - P + 3)P + 7, \ldots, -2, -1, 0, 1, 2,\\
&\ldots, (N - P + 3)P - 7\}.
\end{aligned} \tag{22}$$

Therefore, the uniform DOFs for MISC arrays is:

$$\text{uDOFs} = 2(N - P + 3)P - 13. \tag{23}$$

Substituting (13) into (23) yields

$$\text{uDOFs} = 4N\left\lfloor \frac{N}{4} \right\rfloor - 8\left\lfloor \frac{N}{4} \right\rfloor^2 + 4N - 4\left\lfloor \frac{N}{4} \right\rfloor - 9. \tag{24}$$

Obviously, MISC arrays have closed-form expressions for the achievable number of uniform DOFs with respect to the number of sensors.

Using $N/4$ instead of $\lfloor \frac{N}{4} \rfloor$, (24) can be approximately expressed as

$$\text{uDOFs} \approx \frac{N^2}{2} + 3N - 9. \tag{25}$$

Note that this approximation does not change the orders of magnitude of square term N^2 and linear term N. We can easily show that this approximation is accurate for any even number of $N \geq 5$. For other integers of $N \geq 5$, the difference between the true and approximate uDOFs is between -1.5 and 0.5. More specifically, the number of uniform DOFs can be expressed as

$$\text{uDOFs} = \begin{cases} \frac{N^2}{2} + 3N - 8.5, & N\%4 = 1, \\ \frac{N^2}{2} + 3N - 9, & N\%2 = 0, \\ \frac{N^2}{2} + 3N - 10.5, & N\%4 = 3. \end{cases} \tag{26}$$

For comparison, the uniform DOFs for nested arrays [13] and improved nested arrays [16] are also given by

Nested Arrays:

$$\text{uDOFs} = \begin{cases} \frac{N^2}{2} + N - \frac{1}{2}, & \text{if } N \text{ is odd}, \\ \frac{N^2}{2} + N - 1, & \text{if } N \text{ is even}. \end{cases} \tag{27}$$

Improved Nested Arrays:

$$\text{uDOFs} = \begin{cases} \frac{N^2}{2} + 2N - \frac{7}{2}, & \text{if } N \text{ is odd}, \\ \frac{N^2}{2} + 2N - 3, & \text{if } N \text{ is even}. \end{cases} \tag{28}$$

From (25), (27), (28), we observe that the number of uniform DOFs of the MISC array has the same order of magnitude of N^2 as the nested array and the improved nested array. Moreover, the MISC array has a greater value than the nested array and the improved nested array. Therefore, we can conclude that the MISC array provides a higher number of uniform DOFs than the nested array and the improved nested array. Table I lists the number of uniform DOFs of five kinds of NLAs for a varying number of sensors. It is observed that the nested array has the minimum number of uniform DOFs among all arrays compared in this table. In addition, the improved nested array, ANAI-1 and ANAI-2 offer a higher number of uniform DOFs than the nested array. It is also observed that, when the number of sensors is more than 7, the MISC array provides the highest number of DOFs among all the array configurations compared here. This advantage becomes more evident as the number of sensors increases.

C. Weight Functions

Another advantage of MISC arrays over other sparse arrays is that they are less affected by mutual coupling. It is known that the weight functions at small separations are more important for mutual coupling effects [55]. In particular, the first three weight functions, $w(1)$, $w(2)$ and $w(3)$, have a major impact on the mutual coupling of an array, and $w(1)$ provides the greatest impact [20]. Therefore, in this subsection, we derive the expressions for the first three weight functions of the MISC array to evaluate the mutual coupling effects of MISC arrays.

According to the definition of the weight function and the inter-element spacing set $\mathbb{A}_{\text{MISC}}$, the numbers of elements 1, 2 and 3 in $\mathbb{A}_{\text{MISC}}$ are the weight function $w(1)$, $w(2)$ and $w(3)$, respectively. Therefore, for a MISC array, its weight function

---

$$\begin{aligned}
&\mathbb{D}_1 = \{1, P-2, 2P-2, 3P-2, \ldots, (N-P+1)P-2, (N-P+1)P, (N-P+1)P+2, \ldots, (N-P+2)P-6, \\
&\quad (N-P+2)P-3, (N-P+2)P-1, (N-P+2)P+1, \ldots, (N-P+3)P-7\} \\
&\mathbb{D}_2 = \{P-3, 2P-3, 3P-3, \ldots, (N-P+1)P-3, (N-P+1)P-1, (N-P+1)P+1, \ldots, (N-P+2)P-7, \\
&\quad (N-P+2)P-4, (N-P+2)P-2, (N-P+2)P, \ldots, (N-P+3)P-8\} \\
&\mathbb{D}_3 = \{P, 2P, 3P, \ldots, (N-P)P, (N-P)P+2, (N-P)P+4, \ldots, (N-P+1)P-4, (N-P+1)P-1, \\
&\quad (N-P+1)P+1, (N-P+1)P+3, \ldots, (N-P+2)P-5\} \\
&\mathbb{D}_4 = \{P, 2P, 3P, \ldots, (N-P-1)P, (N-P-1)P+2, (N-P-1)P+4, \ldots, (N-P)P-4, \\
&\quad (N-P)P-1, (N-P)P+1, (N-P)P+3, \ldots, (N-P+1)P-5\} \\
&\ldots\ldots\ldots\ldots\ldots\ldots \\
&\mathbb{D}_{N-P+1} = \{P, 2P, 2P+2, 2P+4, \ldots, 3P-4, 3P-1, 3P+1, 3P+3, \ldots, 4P-5\} \\
&\mathbb{D}_{N-P+2} = \{P, P+2, P+4, \ldots, 2P-4, 2P-1, 2P+1, 2P+3, \ldots, 3P-5\} \\
&\mathbb{D}_{N-P+3} = \{2, 4, \ldots, P-4, P-1, P+1, P+3, \ldots, 2P-5\} \\
&\ldots\ldots\ldots\ldots\ldots\ldots \\
&\mathbb{D}_{N-P+4+(P-4)/2} = \{3, 5, 7, \ldots, P-1\} \\
&\mathbb{D}_{N-P+4+(P-4)/2+1} = \{2, 4, 6, \ldots, P-4\} \\
&\ldots\ldots\ldots\ldots\ldots\ldots \\
&\mathbb{D}_{N-1} = \{2\}
\end{aligned} \tag{21}$$

TABLE I
A SUMMARY OF UNIFORM DOFS OF FIVE KINDS OF NLAS FOR DIFFERENT NUMBER OF SENSORS

Array config.	Number of sensors															
	5	6	7	8	9	10	11	12	13	14	15	16	17	18	19	20
Nested	17	23	31	39	49	59	71	83	97	111	127	143	161	179	199	219
Improved Nested	19	27	35	45	55	67	79	93	107	123	139	157	175	195	215	237
ANAI-1	19	27	35	45	53	65	77	91	103	119	135	153	169	189	209	231
ANAI-2	17	25	33	43	53	65	77	91	105	121	137	155	173	193	213	235
MISC	19	27	35	47	59	71	83	99	115	131	147	167	187	207	227	251

$w(m)$ at $m = 1, 2, 3$ is

$$w(1) = 1,\ w(2) = 2\left\lfloor \frac{N}{4} \right\rfloor - 2,\ w(3) = \begin{cases} 1, \text{ if } N \neq 9, \\ 2, \text{ if } N = 9. \end{cases} \tag{29}$$

In comparison, the first three weight functions for nested arrays [13], coprime arrays [15] and second-order super nested arrays [20] are:

Nested Arrays:

$$w(1) = N_1,\ w(2) = N_1 - 1,\ w(3) = N_1 - 2. \tag{30}$$

Second-Order Super Nested Arrays:

$$w(1) = \begin{cases} 1, \text{ if } N_1 \text{ is odd}, \\ 2, \text{ if } N_1 \text{ is even}, \end{cases} \tag{31}$$

$$w(2) = \begin{cases} N_1 - 1, \text{ if } N_1 \text{ is odd}, \\ N_1 - 3, \text{ if } N_1 \text{ is even}, \end{cases} \tag{32}$$

$$w(3) = \begin{cases} 1, \text{ if } N_1 \text{ is odd}, \\ 3, \text{ if } N_1 = 4, 6, \\ 4, \text{ if } N_1 \text{ is even}, N_1 \geq 8. \end{cases} \tag{33}$$

Coprime Arrays:

$$w(1) = w(2) = w(3) = 2, \tag{34}$$

where N_1, N_2 for nested arrays and M, N for coprime arrays are large enough. For second-order super nested arrays, N_1 and N_2 are integers satisfying $N_1 \geq 4$, $N_2 \geq 3$.

Through $w(1)$, $w(2)$ and $w(3)$, we can roughly compare the mutual coupling effects of the MISC array and the other two sparse arrays with reduced mutual coupling. Specifically, $w(1)$ and $w(3)$ for MISC arrays are always one except the case of $N = 9$, where $w(3)$ is equal to two, whereas $w(1)$, $w(2)$ and $w(3)$ for nested arrays increase as N_1 increases. In addition, the MISC array has smaller values of $w(1)$ and $w(3)$ than those of the coprime array and the second-order super nested array. However, the value of $w(2)$ for MISC arrays will grow with the increase of N. Although the coprime array may have a smaller value of $w(2)$, there are holes in its difference coarray. Therefore, we can conclude from the weight functions that the MISC array is sparser than the nested array and the second-order super nested array, so that the mutual coupling between the elements is greatly reduced.

IV. NUMERICAL EXAMPLES

In this section, we will provide numerical examples to illustrate the superiority of the proposed MISC arrays over the existing sparse arrays in terms of weight functions, mutual coupling matrices, and DOA estimation performance. Note that in all examples, coprime arrays represent extended coprime arrays [24]. In all DOA estimations, for the ULA, the MUSIC algorithm [3] is adopted while for sparse arrays, the spatial smoothing MUSIC algorithm [13], [24], [35] is used to execute DOA estimation. Moreover, we assume that all incident sources have equal power and the number of sources is known. To evaluate the results quantitatively, the root-mean-square error (RMSE) of the estimated normalized DOAs is defined as an average over 1000 independent trials:

$$\text{RMSE} = \sqrt{\frac{1}{1000K} \sum_{i=1}^{1000} \sum_{k=1}^{K} \left(\hat{\bar{\theta}}_k^{(i)} - \bar{\theta}_k \right)^2} \tag{35}$$

where $\hat{\bar{\theta}}_k^{(i)}$ is the estimate of $\bar{\theta}_k$ for the ith trial. Similar to [20], in what follows, we focus on the uniform DOFs, rather than the array aperture, to investigate the overall estimation performance.

A. Weight Functions and Mutual Coupling Matrices

In the first simulation example, we compare the weight functions and mutual coupling matrices of MRA, nested array, coprime array, super nested array ($Q = 2, 3$), ANAI-1, ANAI-2 and MISC array. For all these arrays, we consider three different cases where the number of sensors is 9, 14 and 18, respectively. For the nested array and its derivatives, we set respectively the parameters as $N_1 = 5, N_2 = 4$; $N_1 = N_2 = 7$ and $N_1 = N_2 = 9$. For the coprime array, we choose three sets of parameters, namely, $M = 3, N = 4$; $M = 4, N = 7$ and $M = 5, N = 9$. Moreover, the sensor position sets for the MRAs are given by [23], [56]

$$\begin{aligned} \mathbb{S}_{\text{MRA}} &= \{1, 2, 4, 7, 14, 21, 25, 29, 30\}, \\ \mathbb{S}_{\text{MRA}} &= \{0, 1, 2, 8, 15, 16, 26, 36, 46, 56, 59, 63, 65, 68\}, \\ \mathbb{S}_{\text{MRA}} &= \{0, 1, 2, 5, 10, 15, 26, 37, 48, 59, 70, 81, 92, 98, 104, \\ &\qquad 110, 111, 112\}. \end{aligned} \tag{36}$$

Here, we consider the case with strong mutual coupling [20], [23], where the mutual coupling model (9) is characterized by $c_1 = 0.3e^{j\pi/3}$, $B = 100$, and $c_\ell = c_1 e^{-j(\ell-1)\pi/8}/\ell$ for $2 \leq \ell \leq B$. Fig. 4 shows the weight functions for eight kinds of 14-element NLAs. As shown in Fig. 4, the nested

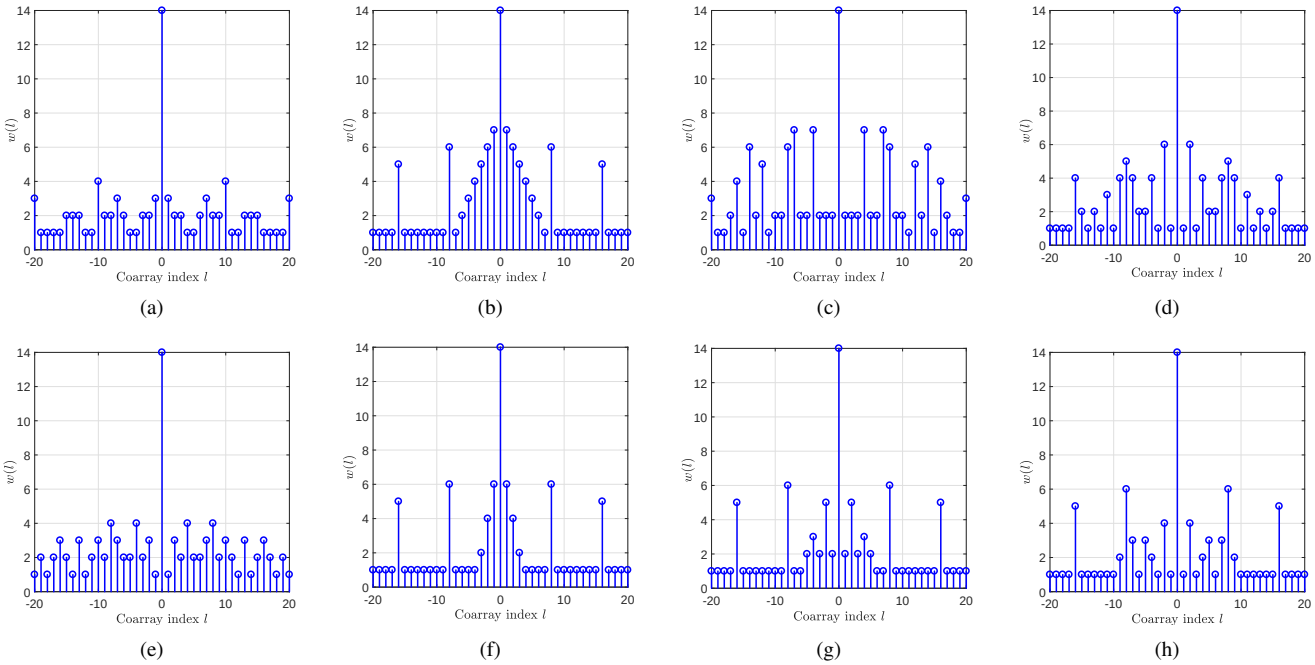

Fig. 4. The weight functions for eight kinds of 14-element NLAs. (a) MRA. (b) Nested. (c) Coprime. (d) Second-order super nested. (e) Third-order super nested. (f) ANAI-1. (g) ANAI-2. (h) MISC.

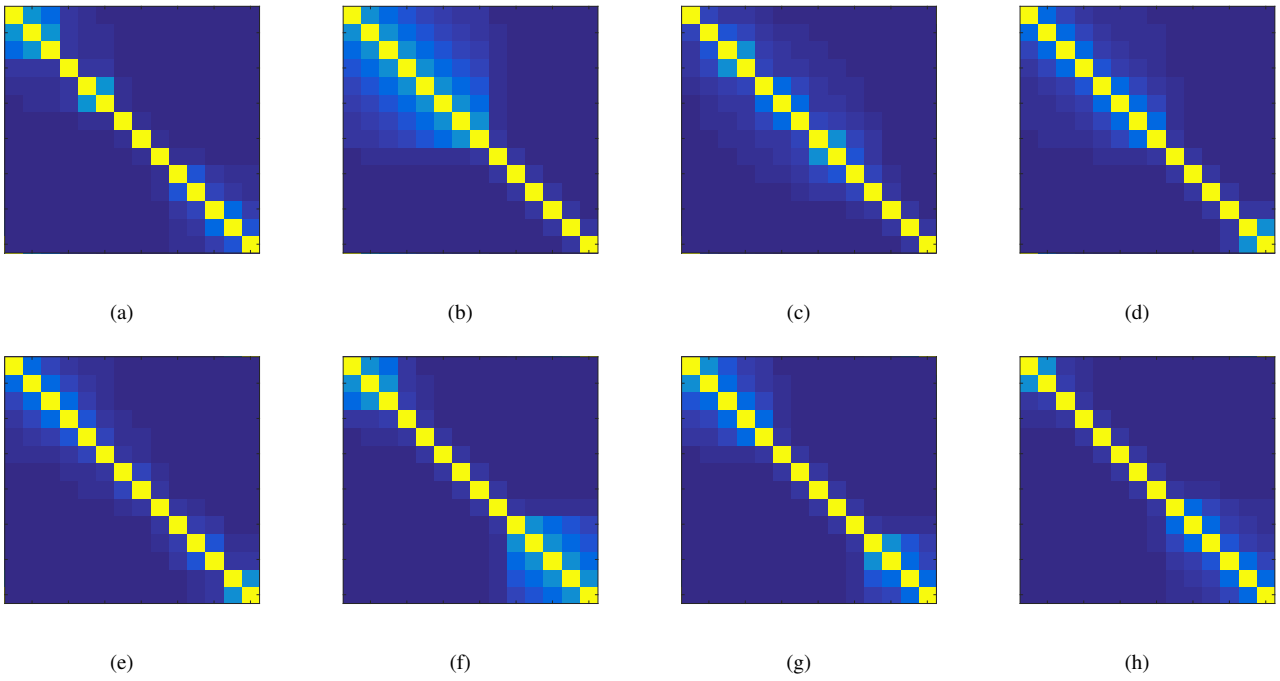

Fig. 5. The magnitudes of the mutual coupling matrices for eight kinds of 14-element NLAs. (a) MRA. (b) Nested. (c) Coprime. (d) Second-order super nested. (e) Third-order super nested. (f) ANAI-1. (g) ANAI-2. (h) MISC.

array exhibits the largest weight functions ($w(1) = 7, w(2) = 6, w(3) = 5$), due to the dense inner ULA. Compared to the nested array, the super nested arrays ($Q = 2, 3$) achieve smaller weight functions ($w(1) = 1, w(2) = 6, w(3) = 1; w(1) = 1, w(2) = 3, w(3) = 2$) by rearranging their dense ULA parts. The coprime array also has smaller weight functions ($w(1) = w(2) = w(3) = 2$) than those of the nested array due to sparser configuration. Both ANAI-1 and ANAI-2 possess smaller weight functions ($w(1) = 6, w(2) = 4, w(3) = 2$; $w(1) = 2, w(2) = 5, w(3) = 2$) than those of the nested array. For the MISC array, the weight functions ($w(1) = 1, w(2) = 4, w(3) = 1$) are even smaller than those of the second-order super nested array. Fig. 5 displays the magnitudes of the mutual coupling matrices for eight kinds of 14-element NLAs. The blue color implies less energy in the corresponding entry. A summary of the weight function and the mutual coupling leakage for eight different NLAs are provided in Table II. It can be seen that the nested array

TABLE II

A SUMMARY OF WEIGHT FUNCTION AND MUTUAL COUPLING LEAKAGE FOR EIGHT KINDS OF NLAS

Array config.	MRA	MISC	Coprime	Nested	Super Nested ($Q=2$)	Super Nested ($Q=3$)	ANAI-1	ANAI-2
9 sensors			$M=3,\ N=4$		$N_1=5, N_2=4$			
$w(1)$	2	1	2	4	2	2	3	2
$w(2)$	1	2	2	3	1	1	1	2
$w(3)$	2	2	4	2	3	3	1	2
L	0.2322	0.1997	0.2589	0.3112	0.2390	0.2390	0.2643	0.2422
14 sensors			$M=4,\ N=7$		$N_1=N_2=7$			
$w(1)$	3	1	2	7	1	1	6	2
$w(2)$	2	4	2	6	6	3	4	5
$w(3)$	2	1	2	5	1	2	2	2
L	0.2248	0.1824	0.2143	0.3333	0.2030	0.1820	0.2982	0.2214
18 sensors			$M=5,\ N=9$		$N_1=N_2=9$			
$w(1)$	4	1	2	9	1	1	8	2
$w(2)$	2	6	2	8	8	5	6	7
$w(3)$	1	1	2	7	1	2	4	2
L	0.2209	0.1802	0.1896	0.3364	0.1979	0.1772	0.3066	0.2121

yields the highest value of L, defined in (12), implying that it suffers from the severest mutual coupling effect. According to the values of L, ANAI-1 and ANAI-2 can moderately reduce the mutual coupling effect, and the super nested array ($Q = 2, 3$) is much less sensitive to the mutual coupling effect. In all cases, the MISC array and the third-order super nested array have the least values of L, indicating that they experience the least mutual coupling effect among all array configurations being compared. More specifically, the third-order super nested array renders a smaller value of L as the number of sensors increases, while the MISC array offers a relatively stable value of L.

B. DOA Estimation in the Absence of Mutual Coupling

In the second simulation example, we compare the DOA estimation performance in the absence of mutual coupling among ULA, MRA, nested array, coprime array, improved nested array, ANAI-1, ANAI-2 and MISC array. The same number of 14 sensors is used for all array configurations. For the improved nested array, we set $N_1 = 6$ and $N_2 = 8$, while the other array configurations are the same as those in Section IV-A.

1) MUSIC Spectra: Fig. 6 shows the MUSIC spectra for eight kinds of 14-element arrays when $K = 50$ sources are located at $\bar{\theta}_k = -0.4 + 0.8(k-1)/49$, $1 \le k \le 50$. The SNR is fixed at 0 dB and the number of snapshots is set as $T = 1000$. It is seen from Fig. 6 that the ULA and the coprime array fail to identify 50 sources due to the limitation in the number of DOFs. The nested array and ANAI-1 have false peaks, while the remaining arrays can resolve 50 true peaks. Furthermore, the MRA and the MISC array exhibit higher peaks than the ANAI-2 and the improved nested array. Therefore, they can provide higher DOA resolution than the ANAI-2 and the improved nested array in the absence of mutual coupling.

2) RMSE Performance: The next simulations consider the RMSE performance versus the input SNR, the number of snapshots, and the number of sources. The fixed parameter setting is $\mathrm{SNR} = 0\,\mathrm{dB}$, $T = 1000$ snapshots, and $K = 20$ sources (except the case where K varies). The sources are located at $\bar{\theta}_k = -0.4 + 0.8(k-1)/(K-1)$, $1 \le k \le K$. Fig. 7 shows the RMSE of the normalized DOA estimates versus the SNR. We see that as the SNR increases, all the RMSEs decrease rapidly except that of the ULA, and attain a steady level when the SNR is higher than -10 dB. Moreover, the MISC array achieves smaller RMSE than the other arrays except the MRA across a wide range of the SNR. Although the MRA provides the best performance, its sensor locations cannot be expressed in a closed form. Fig. 8 illustrates the RMSE of the normalized DOA estimates versus the number of snapshots, all the DOA estimates become more accurate and stabilized as the number of snapshots increases, and the MISC array behaves better than other rivals except the MRA when T is more than 200. Fig. 9 demonstrates the RMSE of the normalized DOA estimates versus the number of sources. As K increases, the DOA estimations of all the arrays suffer performance degradation. But the MISC array owns smaller RMSE than the remaining arrays except the MRA in most cases because it can provide a higher number of uniform DOFs than the arrays. Furthermore, when K is more than 25, the RMSE curve of the ULA will disappear and that of the coprime array will remarkably ascend. The reasons are that $K = 30$ has exceeded the uniform DOFs of the ULA and is close to the uniform DOFs of the coprime array. It is also observed that only the MRA, the MISC array and the improved nested array show stable performance when K varies from 5 to 50. This can be attributed to their advantages in the number of uniform DOFs.

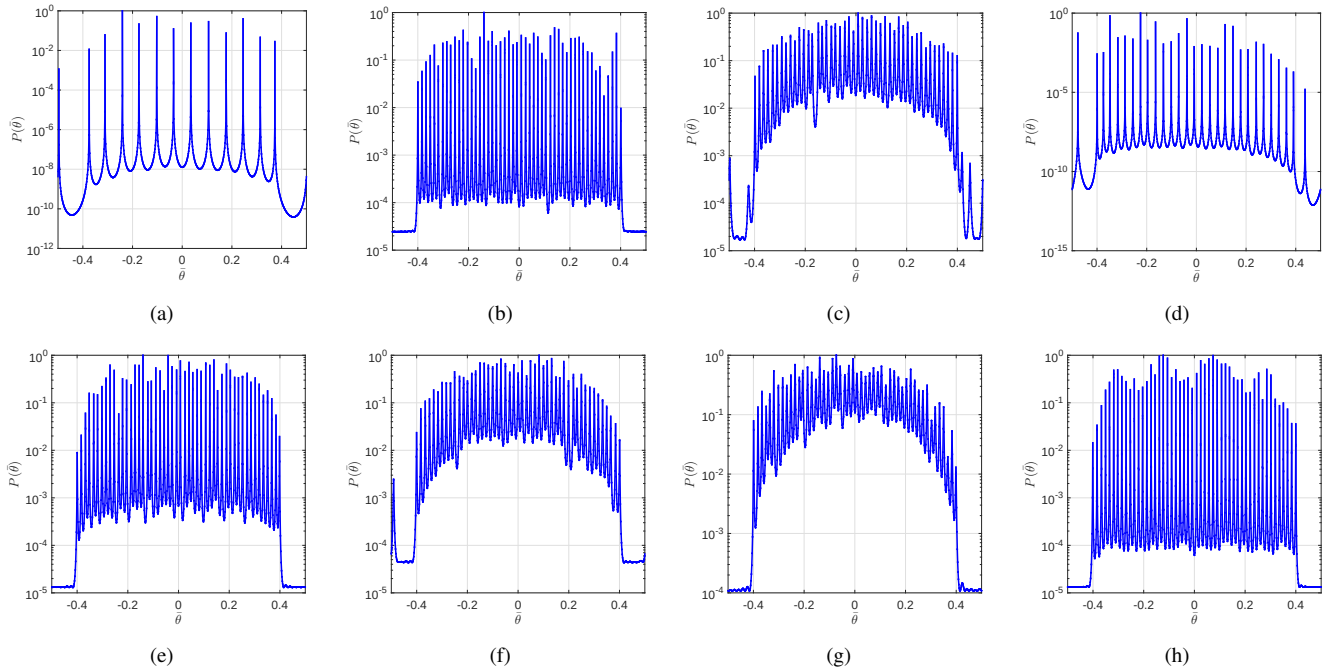

Fig. 6. The MUSIC spectra $P(\bar{\theta})$ for eight kinds of 14-element arrays when $K = 50$ sources are located at $\bar{\theta}_k = -0.4 + 0.8(k-1)/49$, $1 \le k \le 50$. SNR $= 0$ dB and $T = 1000$. (a) ULA. (b) MRA. (c) Nested. (d) Coprime. (e) Improved Nested. (f) ANAI-1. (g) ANAI-2. (h) MISC.

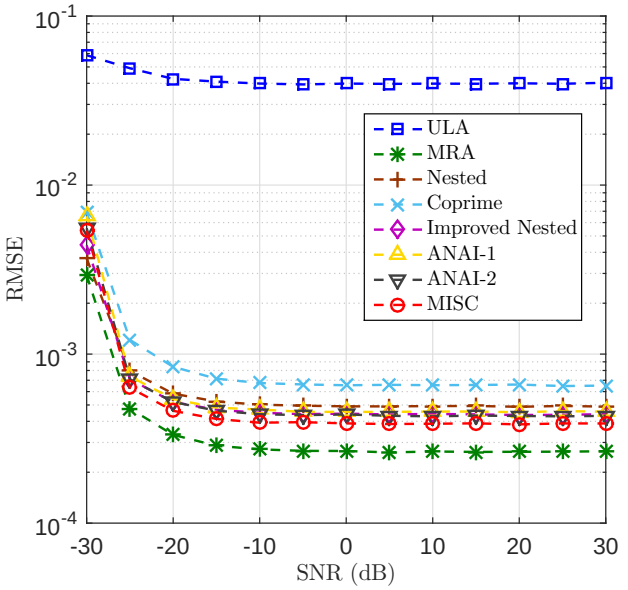

Fig. 7. RMSE of normalized DOA estimates versus the SNR when $K = 20$ sources are located at $\bar{\theta}_k = -0.4+0.8(k-1)/19$, $1 \le k \le 20$. The number of sensors is equal to 14, and the number of snapshots is set as $T = 1000$. Each simulated point is averaged from 1000 trials.

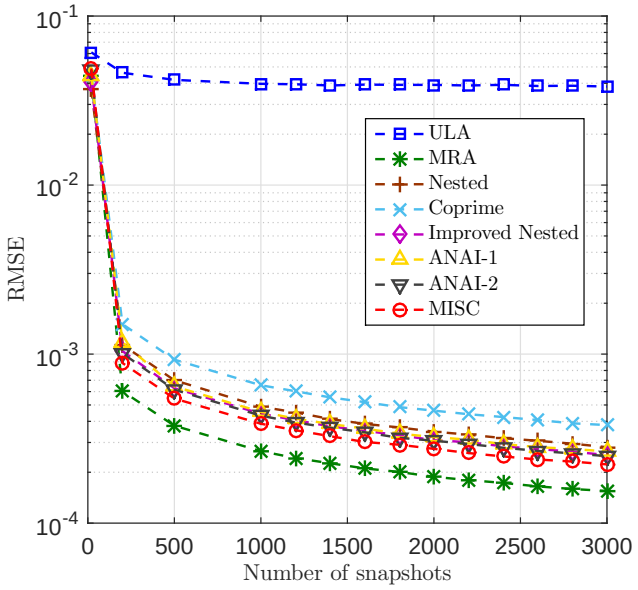

Fig. 8. RMSE of normalized DOA estimates versus the number of snapshots when $K = 20$ sources are located at $\bar{\theta}_k = -0.4+0.8(k-1)/19$, $1 \le k \le 20$. The number of sensors is equal to 14, and the SNR is fixed at 0 dB. Each simulated point is averaged from 1000 trials.

C. DOA Estimation in the Presence of Mutual Coupling

In the third simulation example, we consider eight array configurations: MRA, nested array, coprime array, super nested array ($Q = 2, 3$), ANAI-1, ANAI-2 and MISC array, and then compare their DOA estimation performance in the presence of mutual coupling. The same number of 18 sensors is used for all arrays, whose configurations are the same as those in Section IV-A.

1) MUSIC Spectra: Fig. 10 shows the MUSIC spectra for eight kinds of 18-element arrays when $K = 30$ sources are located at $\bar{\theta}_k = -0.45 + 0.9(k-1)/29$, $1 \le k \le 30$. The SNR is fixed at 0 dB and the number of snapshots is set as $T = 1000$. We observe from Fig. 10 that only the MISC array is capable of detecting all 30 sources, while the other arrays (with false peaks or missing peaks) are not. Since the number of DOFs of these arrays is higher than 30, the MISC array is more effective than the remaining arrays against strong mutual coupling.

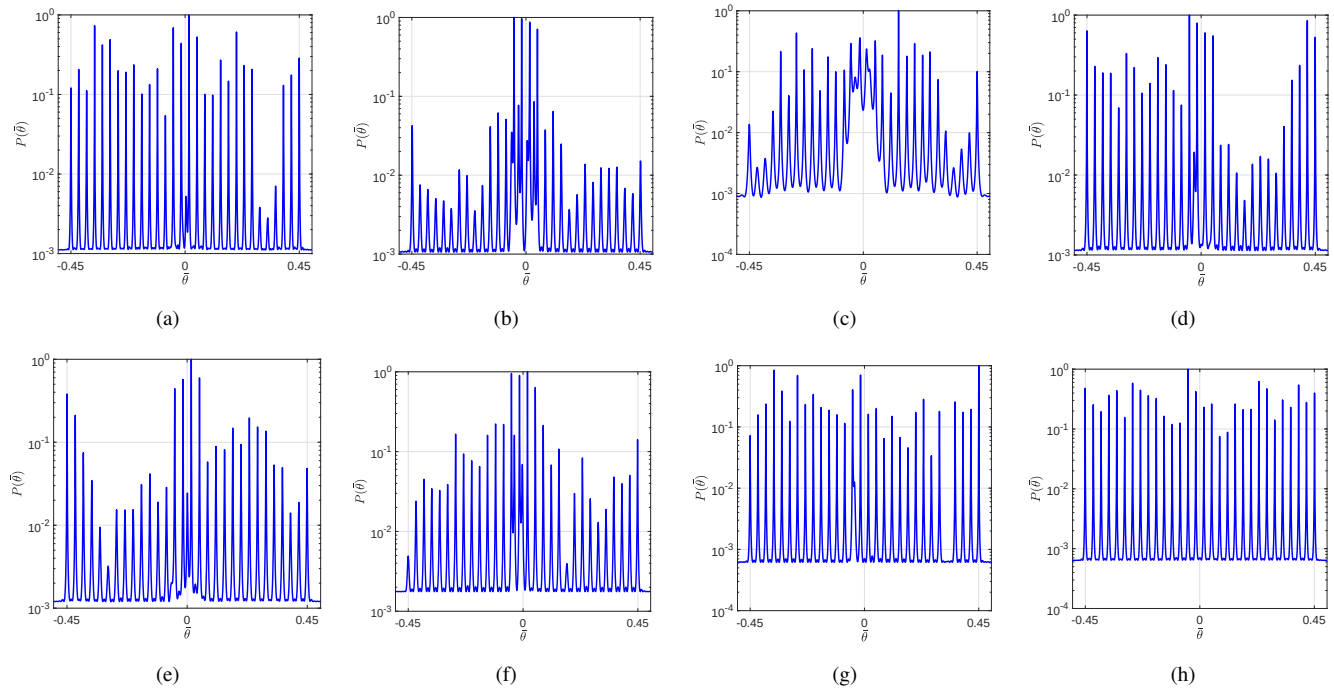

Fig. 10. The MUSIC spectra $P(\bar{\theta})$ for eight kinds of 18-element NLAs when $K = 30$ sources are located at $\bar{\theta}_k = -0.45 + 0.9(k-1)/29$, $1 \le k \le 30$. SNR $= 0$ dB and $T = 1000$. The mutual coupling model (9) is characterized by $c_1 = 0.3e^{j\pi/3}$, $B = 100$, and $c_\ell = c_1 e^{-j(\ell-1)\pi/8}/\ell$ for $2 \le \ell \le B$. (a) MRA. (b) Nested. (c) Coprime. (d) Second-order super nested. (e) Third-order super nested. (f) ANAI-1. (g) ANAI-2. (h) MISC.

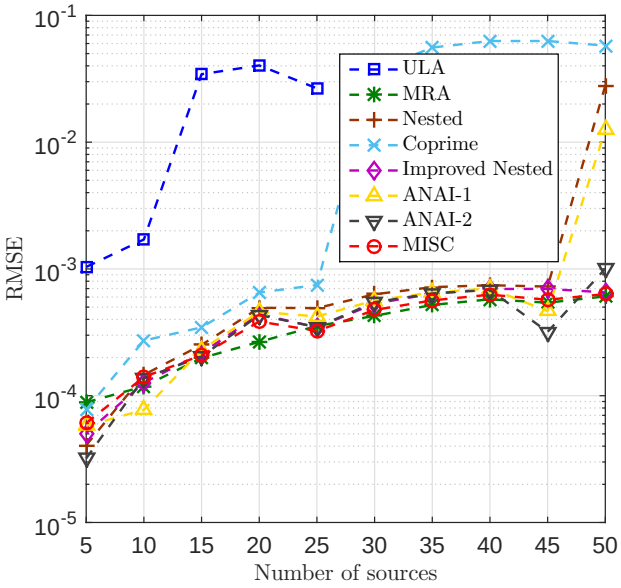

Fig. 9. RMSE of normalized DOA estimates versus the number of sources when K sources are located at $\bar{\theta}_k = -0.4+0.8(k-1)/(K-1)$, $1 \le k \le K$. The number of sensors is 14, SNR $= 0$ dB and $T = 1000$. Each simulated point is averaged from 1000 trials.

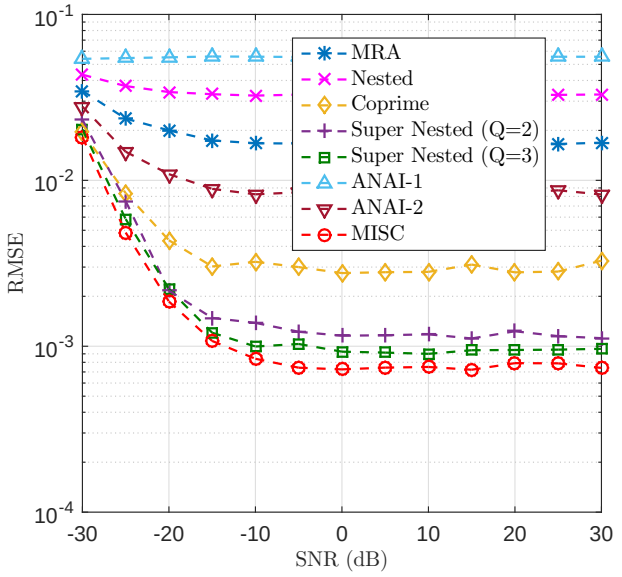

Fig. 11. RMSE of normalized DOA estimates versus the SNR when $K = 25$ sources are located at $\bar{\theta}_k = -0.45 + 0.9(k-1)/24$, $1 \le k \le 25$. The number of sensors is 18 and $T = 1000$. The mutual coupling model (9) is characterized by $c_1 = 0.3e^{j\pi/3}$, $B = 100$, and $c_\ell = c_1 e^{-j(\ell-1)\pi/8}/\ell$ for $2 \le \ell \le B$. Each simulated point is averaged from 1000 trials.

2) RMSE Performance: The next simulations focus on the RMSE performance versus the input SNR, the number of snapshots, the number of sources, and the modulus of coupling coefficient c_1. The mutual coupling model (9) is characterized by $B = 100$, $c_1 = 0.3e^{j\pi/3}$ and $c_\ell = c_1 e^{-j(\ell-1)\pi/8}/\ell$ (except the case where $|c_1|$ varies). The fixed parameter setting is SNR $= 0$ dB, $T = 1000$ snapshots, and $K = 25$ sources (except the case where K varies). The sources are located at $\bar{\theta}_k = -0.45 + 0.9(k-1)/(K-1)$, $1 \le k \le K$.

The RMSE of the normalized DOA estimates versus the SNR is shown in Fig. 11. We see that the MISC array and two super nested arrays exhibit better performance than all the other arrays across a wide range of the SNR, and the MISC array yields the lowest RMSE over the entire SNR range. It indicates that the three arrays outperform the other arrays against

mutual coupling effects and the MISC array is least sensitive to the mutual coupling effects. The RMSE of the normalized DOA estimates versus the number of snapshots is plotted in Fig. 12. It is observed that, as the number of snapshots increases, the RMSE is reduced rapidly for the MISC array and the super nested arrays until T reaches about 1500. In contrast, the RMSE results of the other arrays are reduced rather slowly, especially for the nested array, the coprime array and ANAI-1. Fig. 13 depicts the RMSE of the normalized DOA estimates versus the number of sources. When K is small, the MRA has the minimum RMSE. However, the performance of the MRA will deteriorate rapidly as K increases. In contrast, the performances of the MISC array and the super nested arrays ($Q = 2, 3$) are more stable and begin to evidently deteriorate only when K is more than 20. Additionally, the MISC array will outperform the super nested arrays ($Q = 2, 3$) when K exceeds 25.

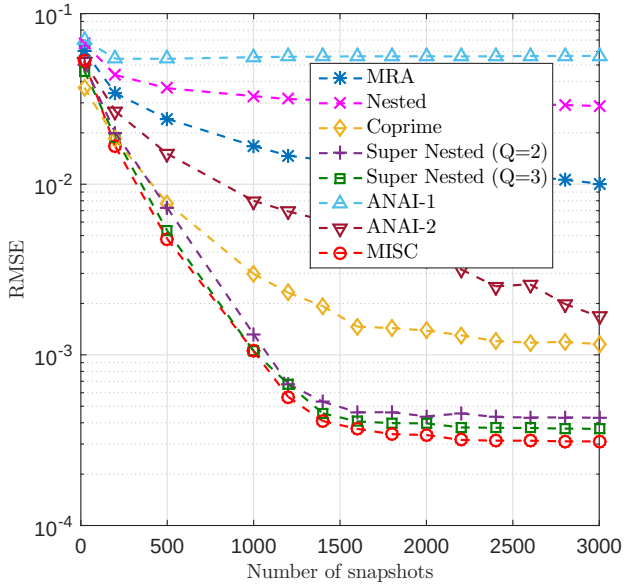

Fig. 12. RMSE of normalized DOA estimates versus the number of snapshots when $K = 25$ sources are located at $\bar{\theta}_k = -0.45 + 0.9(k-1)/24$, $1 \le k \le 25$. The number of sensors is 18, and the SNR is fixed at 0 dB. The mutual coupling model (9) is characterized by $c_1 = 0.3e^{j\pi/3}$, $B = 100$, and $c_\ell = c_1 e^{-j(\ell-1)\pi/8}/\ell$ for $2 \le \ell \le B$. Each simulated point is averaged from 1000 trials.

The RMSE of the normalized DOA estimates versus $|c_1|$ is illustrated in Fig. 14. For any array geometry, along with the increase of $|c_1|$, the corresponding RMSE increases. That is because a higher value of $|c_1|$ introduces more severe mutual coupling effect. When $|c_1|$ is less than 0.2, the MRA yields the best performance while the coprime array achieves the worst performance. The reason for this is that the estimation performance is mainly determine by the number of achievable DOFs when the mutual coupling is weak. Moreover, the MISC array is only slightly worse than the MRA in estimation performance, but works better than the remaining arrays owing to its DOFs advantage. When $|c_1|$ is larger than 0.2, the ANAI-2, the MISC array, and the super nested arrays ($Q = 2, 3$) achieve higher estimation accuracy than the MRA because the estimation accuracy is more severely affected by mutual

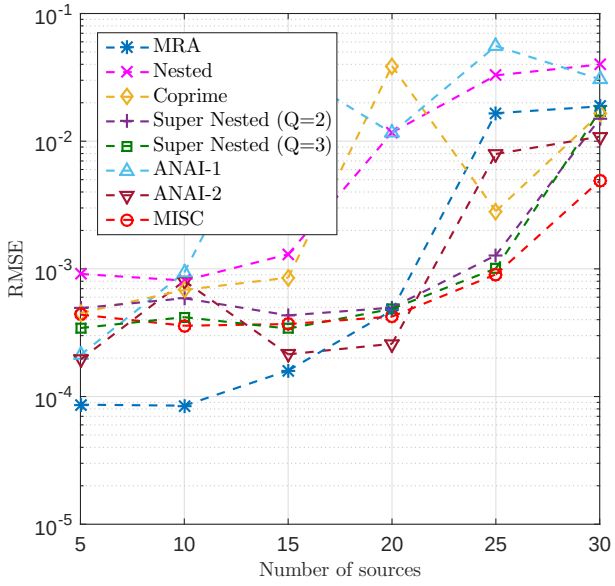

Fig. 13. RMSE of normalized DOA estimates versus the number of sources when K sources are located at $\bar{\theta}_k = -0.45 + 0.9(k-1)/(K-1)$, $1 \le k \le K$. The number of sensors is 18, SNR $= 0$ dB and $T = 1000$. The mutual coupling model (9) is characterized by $c_1 = 0.3e^{j\pi/3}$, $B = 100$, and $c_\ell = c_1 e^{-j(\ell-1)\pi/8}/\ell$ for $2 \le \ell \le B$. Each simulated point is averaged from 1000 trials.

coupling effects in this situation. Furthermore, the MISC array and the third-order super nested array perform better than the ANAI-2 and the second-order super nested array as $|c_1|$ increases because the former two are less sensitive to the mutual coupling effects than the latter two. When $|c_1|$ is greater than 0.5, the coprime array offers smaller RMSE results than other tested arrays. It indicates that the coprime array outperforms other arrays when the mutual coupling is very severe.

V. Conclusions

In this paper, a new NLA configuration, termed MISC arrays, is proposed to simultaneously increase the number of DOFs and reduce the mutual coupling effects. The MISC array is constructed based on an inter-element spacing set, where the maximum inter-element spacing is analytically specified. More specifically, for a given number of sensors, the sensor locations and the number of DOFs of a MISC array are uniquely determined and can be expressed by closed-form expressions. Theoretical derivations show that MISC arrays have hole-free difference coarrays and can provide a higher number of DOFs than nested arrays and improved nested arrays. Furthermore, MISC arrays are less sensitive to mutual coupling effects as compared to coprime arrays and second-order super nested arrays. Numerical results verify that the MISC array is superior to the existing NLAs in terms of weight functions, mutual coupling matrices as well as DOA estimation performance.

References

[1] H. Krim and M. Viberg, "Two decades of array signal processing research: The parametric approach," *IEEE Signal Process. Mag.*, vol. 13, no. 4, pp. 67–94, July 1996.

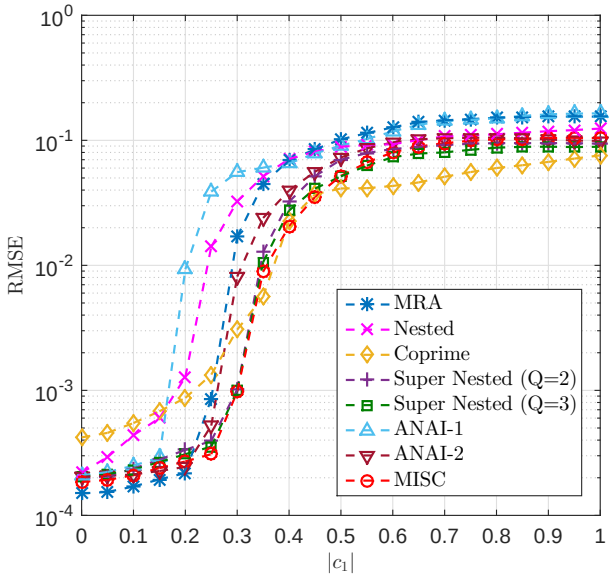

Fig. 14. RMSE of normalized DOA estimates versus $|c_1|$ when $K = 25$ sources are located at $\bar{\theta}_k = -0.45+0.9(k-1)/24$, $1 \le k \le 25$. The number of sensors is 18, SNR $= 0$ dB and $T = 1000$. The mutual coupling model (9) is characterized by $c_1 = |c_1|e^{j\pi/3}$, $B = 100$, and $c_\ell = c_1 e^{-j(\ell-1)\pi/8}/\ell$ for $2 \le \ell \le B$. Each simulated point is averaged from 1000 trials.

[2] H. L. Van Trees, *Detection, Estimation, and Modulation Theory, Part IV: Optimum Array Processing*. New York: Wiley, 2002.

[3] R. Schmidt, "Multiple emitter location and signal parameter estimation," *IEEE Trans. Antennas Propag.*, vol. 34, no. 3, pp. 276–280, Mar. 1986.

[4] R. Roy and T. Kailath, "ESPRIT-estimation of signal parameters via rotational invariance techniques," *IEEE Trans. Acoust., Speech, Signal Process.*, vol. 37, no. 7, pp. 984–995, July 1989.

[5] R. T. Hoctor and S. A. Kassam, "The unifying role of the coarray in aperture synthesis for coherent and incoherent imaging," *Proc. IEEE*, vol. 78, no. 4, pp. 735–752, Apr. 1990.

[6] E. BouDaher, F. Ahmad, M. G. Amin, and A. Hoorfar, "Mutual coupling effect and compensation in non-uniform arrays for direction-of-arrival estimation," *Digital Signal Process.*, vol. 61, pp. 3–14, Feb. 2017.

[7] A. Moffet, "Minimum-redundancy linear arrays," *IEEE Trans. Antennas Propag.*, vol. 16, no. 2, pp. 172–175, Mar. 1968.

[8] S. U. Pillai, Y. Bar-Ness, and F. Haber, "A new approach to array geometry for improved spatial spectrum estimation," *Proc. IEEE*, vol. 73, no. 10, pp. 1522–1524, Oct. 1985.

[9] S. Pillai and F. Haber, "Statistical analysis of a high resolution spatial spectrum estimator utilizing an augmented covariance matrix," *IEEE Trans. Acoust., Speech, Signal Process.*, vol. 35, no. 11, pp. 1517–1523, Nov. 1987.

[10] G. S. Bloom and S. W. Golomb, "Applications of numbered undirected graphs," *Proc. IEEE*, vol. 65, no. 4, pp. 562–570, Apr. 1977.

[11] D. A. Linebarger, I. H. Sudborough, and I. G. Tollis, "Difference bases and sparse sensor arrays," *IEEE Trans. Inf. Theory*, vol. 39, no. 2, pp. 716–721, Mar. 1993.

[12] P. Pal and P. P. Vaidyanathan, "A novel array structure for directions-of-arrival estimation with increased degrees of freedom," in *Proc. IEEE International Conference on Acoustics, Speech and Signal Processing (ICASSP)*, Dallas, TX, USA, Mar. 2010, pp. 2606–2609.

[13] ——, "Nested arrays: A novel approach to array processing with enhanced degrees of freedom," *IEEE Trans. Signal Process.*, vol. 58, no. 8, pp. 4167–4181, Aug. 2010.

[14] P. P. Vaidyanathan and P. Pal, "Sparse sensing with coprime arrays," in *Proc. Asilomar Conf. Signals, Syst., Comput. (Asilomar)*, Pacific Grove, CA, USA, Nov. 2010, pp. 1405–1409.

[15] ——, "Sparse sensing with co-prime samplers and arrays," *IEEE Trans. Signal Process.*, vol. 59, no. 2, pp. 573–586, Feb. 2011.

[16] M. Yang, L. Sun, X. Yuan, and B. Chen, "Improved nested array with hole-free DCA and more degrees of freedom," *Electron. Lett.*, vol. 52, no. 25, pp. 2068–2070, Dec. 2016.

[17] P. Pal and P. P. Vaidyanathan, "Nested arrays in two dimensions, Part I: Geometrical considerations," *IEEE Trans. Signal Process.*, vol. 60, no. 9, pp. 4694–4705, Sep. 2012.

[18] ——, "Nested arrays in two dimensions, Part II: Application in two dimensional array processing," *IEEE Trans. Signal Process.*, vol. 60, no. 9, pp. 4706–4718, Sep. 2012.

[19] C. L. Liu and P. P. Vaidyanathan, "Super nested arrays: Sparse arrays with less mutual coupling than nested arrays," in *Proc. IEEE International Conference on Acoustics, Speech and Signal Processing (ICASSP)*, Shanghai, China, Mar. 2016, pp. 2976–2980.

[20] ——, "Super nested arrays: Linear sparse arrays with reduced mutual coupling–Part I: Fundamentals," *IEEE Trans. Signal Process.*, vol. 64, no. 15, pp. 3997–4012, Aug. 2016.

[21] ——, "High order super nested arrays," in *Proc. IEEE Sensor Array Multichannel Signal Processing Workshop*, Rio de Janerio, Brazil, July 2016, pp. 1–5.

[22] ——, "Super nested arrays: Linear sparse arrays with reduced mutual coupling–Part II: High-order extensions," *IEEE Trans. Signal Process.*, vol. 64, no. 16, pp. 4203–4217, Aug. 2016.

[23] J. Liu, Y. Zhang, Y. Lu, S. Ren, and S. Cao, "Augmented nested arrays with enhanced DOF and reduced mutual coupling," *IEEE Trans. Signal Process.*, vol. 65, no. 21, pp. 5549–5563, Nov. 2017.

[24] P. Pal and P. P. Vaidyanathan, "Coprime sampling and the MUSIC algorithm," in *Proc. Digital Signal Processing Workshop and IEEE Signal Processing Education Workshop (DSP/SPE)*, Sedona, AZ, USA, Jan. 2011, pp. 289–294.

[25] S. Qin, Y. D. Zhang, and M. G. Amin, "Generalized coprime array configurations," in *Proc. IEEE Sensor Array Multichannel Signal Processing Workshop*, A Coruna, Spain, Jun. 2014, pp. 529–532.

[26] ——, "Generalized coprime array configurations for direction-of-arrival estimation," *IEEE Trans. Signal Process.*, vol. 63, no. 6, pp. 1377–1390, Mar. 2015.

[27] D. Bush and N. Xiang, "n-tuple coprime sensor arrays," *J. Acoust. Soc. Am.*, vol. 142, no. EL567, 2017.

[28] S. A. Alawsh and A. H. Muqaibel, "Multi-level prime array for sparse sampling," *IET Signal Process.*, vol. 12, no. 6, pp. 688–699, Aug. 2018.

[29] P. Pal and P. P. Vaidyanathan, "Multiple level nested array: An efficient geometry for $2q$th order cumulant based array processing," *IEEE Trans. Signal Process.*, vol. 60, no. 3, pp. 1253–1269, Mar. 2012.

[30] K. Han and A. Nehorai, "Wideband Gaussian source processing using a linear nested array," *IEEE Signal Process. Lett.*, vol. 20, no. 11, pp. 1110–1113, Nov. 2013.

[31] ——, "Improved source number detection and direction estimation with nested arrays and ULAs using jackknifing," *IEEE Trans. Signal Process.*, vol. 61, no. 23, pp. 6118–6128, Dec. 2013.

[32] Z. Weng and P. M. Djuri, "A search-free DOA estimation algorithm for coprime arrays," *Digital Signal Process.*, vol. 24, pp. 27–33, Jan. 2014.

[33] K. Han and A. Nehorai, "Nested array processing for distributed sources," *IEEE Signal Process. Lett.*, vol. 21, no. 9, pp. 1111–1114, Sep. 2014.

[34] Z. Tan, Y. C. Eldar, and A. Nehorai, "Direction of arrival estimation using co-prime arrays: A super resolution viewpoint," *IEEE Trans. Signal Process.*, vol. 62, no. 21, pp. 5565–5576, Nov. 2014.

[35] C. L. Liu and P. P. Vaidyanathan, "Remarks on the spatial smoothing step in coarray MUSIC," *IEEE Signal Process. Lett.*, vol. 22, no. 9, pp. 1438–1442, Sep. 2015.

[36] S. Qin, Y. D. Zhang, M. G. Amin, and B. Himed, "DOA estimation exploiting a uniform linear array with multiple co-prime frequencies," *Signal Process.*, vol. 130, pp. 37–46, Jan. 2017.

[37] M. Wang and A. Nehorai, "Coarrays, MUSIC, and the Cramér-Rao bound," *IEEE Trans. Signal Process.*, vol. 65, no. 4, pp. 933–946, Feb. 2017.

[38] M. G. Amin, P. P. Vaidyanathan, Y. D. Zhang, and P. Pal, "Editorial for coprime special issue," *Digital Signal Process.*, vol. 61, pp. 1–2, Feb. 2017.

[39] C.-L. Liu and P. Vaidyanathan, "Cramér-Rao bounds for coprime and other sparse arrays, which find more sources than sensors," *Digital Signal Process.*, vol. 61, pp. 43–61, Feb. 2017.

[40] Z. Shi, C. Zhou, Y. Gu, N. A. Goodman, and F. Qu, "Source estimation using coprime array: A sparse reconstruction perspective," *IEEE Sensors J.*, vol. 17, no. 3, pp. 755–765, Feb. 2017.

[41] C. Zhou, Y. Gu, Y. D. Zhang, Z. Shi, T. Jin, and X. Wu, "Compressive sensing-based coprime array direction-of-arrival estimation," *IET Communications*, vol. 11, no. 11, pp. 1719–1724, Aug. 2017.

[42] J. Shi, G. Hu, X. Zhang, F. Sun, and H. Zhou, "Sparsity-based two-dimensional DOA estimation for coprime array: From sumdifference coarray viewpoint," *IEEE Trans. Signal Process.*, vol. 65, no. 21, pp. 5591–5604, Nov. 2017.

[43] Y. Liu and J. R. Buck, "Gaussian source detection and spatial spectral estimation using a coprime sensor array with the min processor," *IEEE Trans. Signal Process.*, vol. 66, no. 1, pp. 186–199, Jan. 2018.
[44] C. Zhou, Y. Gu, X. Fan, Z. Shi, G. Mao, and Y. D. Zhang, "Direction-of-arrival estimation for coprime array via virtual array interpolation," *IEEE Trans. Signal Process.*, vol. 66, no. 22, pp. 5956–5971, Nov. 2018.
[45] C. Zhou, Y. Gu, Z. Shi, and Y. D. Zhang, "Off-grid direction-of-arrival estimation using coprime array interpolation," *IEEE Signal Process. Lett.*, vol. 25, no. 11, pp. 1710–1714, Nov. 2018.
[46] I. Gupta and A. Ksienski, "Effect of mutual coupling on the performance of adaptive arrays," *IEEE Trans. Antennas Propag.*, vol. 31, no. 5, pp. 785–791, Sep. 1983.
[47] B. Friedlander and A. J. Weiss, "Direction finding in the presence of mutual coupling," *IEEE Trans. Antennas Propag.*, vol. 39, no. 3, pp. 273–284, Mar. 1991.
[48] T. Svantesson, "Modeling and estimation of mutual coupling in a uniform linear array of dipoles," in *Proc. IEEE International Conference on Acoustics, Speech and Signal Processing (ICASSP)*, Phoenix, AZ, USA, Mar. 1999, pp. 2961–2964.
[49] ——, "Direction finding in the presence of mutual coupling," Master's thesis, Chalmers Univ. Technol., Chalmers, Sweden, 1999.
[50] ——, "Mutual coupling compensation using subspace fitting," in *Proc. IEEE Sensor Array Multichannel Signal Processing Workshop*, Cambridge, MA, USA, Mar. 2000, pp. 494–498.
[51] F. Sellone and A. Serra, "A novel online mutual coupling compensation algorithm for uniform and linear arrays," *IEEE Trans. Signal Process.*, vol. 55, no. 2, pp. 560–573, Feb. 2007.
[52] Z. Ye, J. Dai, X. Xu, and X. Wu, "DOA estimation for uniform linear array with mutual coupling," *IEEE Trans. Aerosp. Electron. Syst.*, vol. 45, no. 1, pp. 280–288, Jan. 2009.
[53] B. Liao, Z. G. Zhang, and S. C. Chan, "DOA estimation and tracking of ulas with mutual coupling," *IEEE Trans. Aerosp. Electron. Syst.*, vol. 48, no. 1, pp. 891–905, Jan. 2012.
[54] U. V. Dias and S. Srirangarajan, "Co-prime arrays and difference set analysis," in *Proc. 25th European Signal Processing Conference (EUSIPCO)*, Kos, Greece, Aug. 2017, pp. 931–935.
[55] C. L. Liu and P. P. Vaidyanathan, "Hourglass arrays and other novel 2-D sparse arrays with reduced mutual coupling," *IEEE Trans. Signal Process.*, vol. 65, no. 13, pp. 3369–3383, July 2017.
[56] M. Ishiguro, "Minimum redundancy linear arrays for a large number of antennas," *Radio Sci.*, vol. 15, no. 6, pp. 1163–1170, Nov. 1980.

Zhi Zheng (M'11) received the M.S. and Ph.D. degrees in electronic engineering and information & communication engineering from the University of Electronic Science and Technology of China (UESTC), Chengdu, China, in 2007 and 2011, respectively. From 2014 to 2015, he was an Academic Visitor with the Department of Electrical and Electronic Engineering, Imperial College London, U.K. Since 2011, he has been with the School of Information and Communication Engineering, UESTC, where he is currently an Associate Professor. His research interests lie in the areas of statistical and array signal processing, including direction finding, source localization, target tracking, sparse array design, robust adaptive beamforming, jammer suppression, compressive sensing, machine learning, and convex optimization, with applications to radar, sonar, satellite navigation, wireless communications, wireless sensor networks, etc.

Wen-Qin Wang (M'08-SM'16) received the B.S. degree in electrical engineering from Shandong University, Shandong, China, in 2002, the M.E. and Ph.D. degrees in information and communication engineering from the University of Electronic Science and Technology of China (UESTC), Chengdu, China, in 2005 and 2010, respectively.

From 2005 to 2007, he was with the National Key Laboratory of Microwave Imaging Technology, Chinese Academy of Sciences, Beijing, China. From 2011 to 2012, he was a Visiting Scholar with the Stevens Institute of Technology, NJ, USA. From 2012 to 2013, he was a Hong Kong Scholar with the City University of Hong Kong, Hong Kong. From 2014 to 2016, he was a Marie Curie Fellow with the Imperial College London, U.K. Since 2007, he has been with the School of Information and Communication Engineering, UESTC, where he is currently a Professor and the Director of Multi-Dimensional Information Sensing and Processing Research Centre. His research interests span the area of array signal processing and circuit systems for radar, communications and microwave remote sensing.

He was the recipient of the Marie Curie International Incoming Fellowship, the National Young Top-Notch Talent of the Ten-Thousand Talent Program Award, and the Hong Kong Scholar Fellowship. He is an editorial board member of four international journals.

Yangyang Kong was born in Chongqing, China, in 1993. He received the B.S. degree in information and computing science from the Chongqing University of Posts and Telecommunications, Chongqing, China, in 2015, and M.S. degree in communication and information system from the University of Electronic Science and Technology of China, Chengdu, China, in 2018. His current research interests include array signal processing, statistical signal processing, compressive sensing, machine learning, convex optimization, signal processing for communications, MIMO communications, wireless sensor networks, etc.

Yimin D. Zhang (F'19) received his Ph.D. degree from the University of Tsukuba, Tsukuba, Japan, in 1988. He is currently an Associate Professor at the Department of Electrical and Computer Engineering, College of Engineering, Temple University, Philadelphia, PA. From 1998 to 2015, he was a research faculty at the Center for Advanced Communications, Villanova University, Villanova, PA. His research interests lie in the areas of statistical signal and array processing, including compressive sensing, machine learning, convex optimization, timefrequency analysis, MIMO systems, radar imaging, direction finding, target localization and tracking, wireless and cooperative networks, and jammer suppression, with applications to radar, wireless communications, and satellite navigation. He has published more than 340 journal and conference papers and 14 book chapters in these areas.

Dr. Zhang is an Associate Editor for the IEEE TRANSACTIONS ON SIGNAL PROCESSING and an Editor for the Signal Processing journal. He was an Associate Editor for the IEEE SIGNAL PROCESSING LETTERS during 20062010, and an Associate Editor for the Journal of the Franklin Institute during 20072013. He is a member of the Sensor Array and Multichannel Technical Committee and the Signal Processing Theory and Methods Technical Committee of the IEEE Signal Processing Society. He was the Technical Co-Chair of the 2018 IEEE Sensor Array and Multichannel Signal Processing Workshop. He received the 2016 IET Radar, Sonar & Navigation Premium Award and the 2017 IEEE Aerospace and Electronic Systems Society Harry Rowe Mimno Award, and coauthored a paper that received the 2018 IEEE Signal Processing Society Young Author Best Paper Award.